Articles

Video Microscopy Study of the Potential Energy of a Colloidal Particle Confined between Two Plates

Grace Martinelli Kepler† and Seth Fraden*

Martin Fisher School of Physics, Brandeis University, Waltham, Massachusetts 02254

Received September 29, 1993. In Final Form: March 8, 1994®

Using video microscopy techniques, we have measured the position distribution of polystyrene spheres [$P(z)$] suspended in deionized water and confined between two glass plates. The sphere–plate interaction potential [$U(z)$] was deduced using equilibrium statistical mechanics: $P(z) = C \exp[-U(z)/k_BT]$. Measurements are presented for five different values of the plate spacing, and the results show that the rms displacement of the spheres, perpendicular to the plates, increases exponentially as the gap increases. The average position of the spheres is not always located at the midplane of the gap, indicating that there may be variations in the surface charge of the two glass plates. A comparison is made with the theory of Derjaguin, Landau, Verwey, and Overbeek (DLVO) for the interaction of colloidal particles with plane surfaces, and the experimental results are shown to be consistent with a harmonic approximation to the theory.

Introduction

The measurement of statistical distribution functions in colloidal suspensions using direct microscopic observation has a long history, and the first quantitative investigations of Brownian motion were performed this way.[1] Here we study the motion of a single charged sphere confined between two glass plates using digital video light microscopy and measure the distribution of the positions in the direction perpendicular (z) to the plates. The aim of the measurement is to determine the interaction potential $U(z)$, which is related to the equilibrium distribution function by

$$P(z) = Ce^{-U(z)/k_BT} \quad (1)$$

with C a normalization constant. The interaction potential of a single sphere with a single plate has been determined through the measurement of the displacement distribution function using a technique based on the frustrated total internal reflection of light.[2] However, the great sensitivity of this technique, which arises from the exponential dependence of transmitted light as a function of sphere–plate separation, also limits its range to the order of a skin depth of light. A second method, utilizing a colloidal particle attached to an atomic force microscope, also provides high-resolution data for the interaction forces between a spherical particle and a glass plate.[3] In contrast, direct microscopic observation works best for particles with separations of at least the wavelength of light, and thus can be used to study spheres with a large sphere–plate separation. In addition, this technique is not restricted to the sphere–plate geometry, but can be used to study the interparticle potential between colloidal particles in a colloidal suspensions. This latter case will be the subject of a different paper.[4]

This paper has two goals. The first is to test the feasibility of the method of measuring distribution functions using direct microscopic observation to obtain the interaction potential. The second goal is to study the magnitude of the fluctuations of colloidal particles confined between two glass plates. This geometry has been used in studies of two-dimensional melting of colloidal crystals, where the colloid is confined to a single thin layer by the two plates.[5] By increasing the spacing of the plates, a low ionic strength dispersion can change from a 2D dilute gas to a highly-ordered single-layer crystal. Although the motion of the spheres is mostly in a plane parallel to the plates, there is some motion in the direction perpendicular to the plates and, as the gap is increased, the motion of the spheres out of the plane becomes larger until two layers of spheres can be accommodated. The interaction of individual spheres with the confirming surfaces has not, to our knowledge, been studied.

In this paper, we present experimental measurements, using video microscopy, of the movement of the spheres in the direction perpendicular to the confining plates for five different plate spacings. It is found that the sphere distributions obtained from the data are well described by Gaussian distributions, which broaden as the gap is widened. The Gaussian shape of the distributions and the functional form of the broadening, as the gap is increased, is consistent with a harmonic approximation to the DLVO theory of sphere–surface interactions, using only screened electrostatic interactions.

Experimental Procedure

The 2D cell consists of a silicone o-ring sandwiched between two pieces of 1-in. × 1-in. microscope slide glass. A small glass post ($^1/_8$ in. × $^1/_8$ in. × $^1/_{16}$ in.) is glued to one

* To whom correspondence should be sent.
† Current address CIIT, P.O. Box 12137, Research Triangle Park, NC 27709.

® Abstract published in *Advance ACS Abstracts*, June 15, 1994.

(1) Chandrasekhar, S. *Rev. Mod. Phys.* **1943**, *15*, 1.
(2) Prieve, D. C.; Frej, N. A. *Langmuir* **1990**, *6*, 396. Brown, M. A.; Staples, E. J. *Langmuir* **1990**, *6*, 1260. Flicker, S. G.; Tipa, J. L.; Bike, S. G. *J. Collect. Int. Sci.* **1993**, *158*, 317.
(3) Ducker, W. A.; Senden, T. J.; Pashley, R. M. *Nature* **1991**, *353*, 239. Ducker, W. A.; Senden, T. J.; Pashley, R. M. *Langmuir* **1992**, *8*, 1831.
(4) Kepler, G. M.; Fraden, S. *Phys. Rev. Lett.*, to be published.
(5) Murray, C. A.; Van Winkle, D. H. *Phys. Rev. Lett.* **1987**, *58*, 1200. Murray, C. A.; Van Winkle, D. H.; Wenk, R. A. *Phase Transitions* **1990**, *21*, 93. Murray, C. A.; Sprenger, W. O.; Wenk, R. A. *Phys. Rev. B* **1990**, *42*, 688.

0743-7463/94/2410-2501$04.50/0

of the glass windows with transparent Norland optical adhesive, and the o-ring is compressed to produce a small gap between the post and the glass window. Data was taken for five different gaps: 4.0, 5.0, 6.2, 7.2, and 8.4 μm, in that order.

The thicknesses of the gaps were measured using a laser interference method described by Hurd.[6] The accuracy of the measurements is limited by the fact that the beam samples different parts of the gap as the cell is rotated for the measurements, and any nonparallelism will result in a measurement which is an average of the sampled area. During assembly the plates were adjusted for parallelism with a monochromatic light source, and for these experiments the thickness measurements are expected to be accurate to within 0.14 μm, the maximum variation of the thickness from the center to the outside edge of the post.

The cell is filled with a dilute colloidal dispersion of 1.27-μm polystyrene spheres in a density matching 50:50 mixture of D_2O and H_2O. Deionizing resin is present in the cell, but outside the gap, to maintain the low ionic concentration of the dispersion.

The spheres are viewed with an Olympus microscope, with a 40× objective and long working length condenser, operated in transmission mode. A CCD camera mounted on the microscope records images that are digitized and analyzed on a mainframe computer.

When properly focused the spheres appear as dark objects on a brighter background. However, a polystyrene sphere acts as a lens and by slightly defocusing can be made to appear as a bright disk surrounded by a dark annulus and background. This optical property is exploited in the particle detection algorithm, where an intensity threshold is used. The threshold value is chosen to be greater than the intensity of the dark annulus and background, but less than the intensity of the bright disk. Each line of the digitized image is then scanned for pixels that are above the threshold value. When such a pixel is encountered, the neighboring pixels are checked. If any are above threshold, the process is repeated. With reasonable adjustment of the threshold, "clusters" of contiguous bright pixels are found, which identify sphere centers. Once the clusters are located, the particle position is determined from the center-of-intensity of the cluster.

By using the sphere position obtained in this way, a total intensity (I) is calculated by summing the intensities of pixels in an array centered on the sphere. The size of the array is chosen so that, at its maximum, the entire bright disk is contained within the array. In this way the pixels at the edge of the cluster, which may fluctuate about the threshold intensity, do not cause large fluctuations in the overall particle intensity.

The size and intensity of the bright disk is a function of the displacement of the sphere relative to the focal plane of the objective. The intensity of the disk is a maximum when the refracted light from the sphere is focused in the focal plane of the objective. As the sphere moves in either direction away from this position the intensity of the disk decreases.

Using a reference sphere stuck to one of the glass surfaces and changing the position of the focal plane (stage height), we can determine the disk intensity as a function of the displacement from the position of maximum intensity. These displacements are in a direction perpendicular to the confining plates.

When a moving sphere is tracked the focal plane is held constant, but the sphere position relative to the focal plane is changing. By measuring the intensity of the moving

(6) Hurd, A. The Lattice Dynamics of Colloidal Crystals. Ph.D. Thesis, University of Colorado, Boulder, 1981.

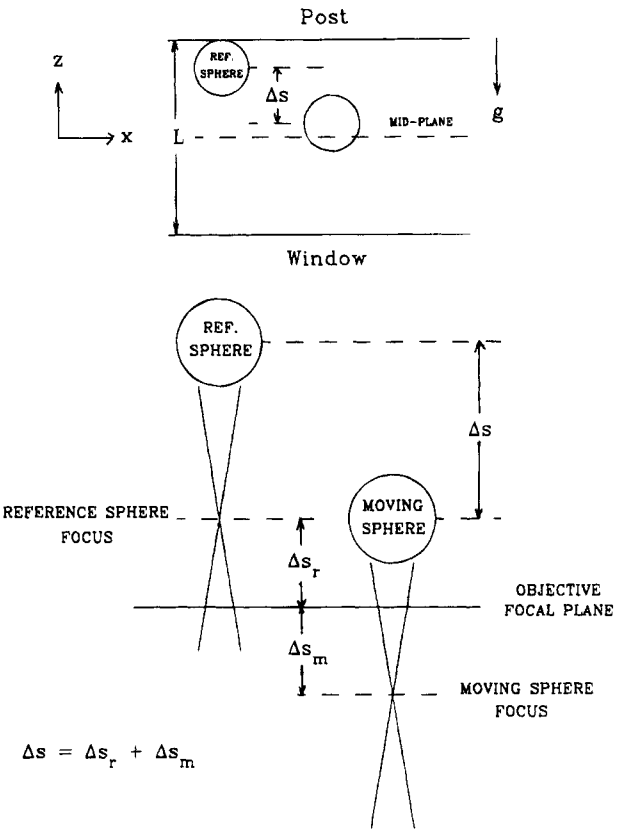

Figure 1. Schematic diagram of the experimental situation. Incident light is focused by the spheres. The focal plane of the objective lies between the focal points of the reference and moving spheres so that both can be located by the particle detection algorithm. The intensity of the spheres is a function of the displacement from the focal plane of the objective. The relative displacement of the reference and moving sphere can be determined using their intensities and the calibration curve of Figure 2. The displacement of the moving sphere from the midplane of the gap is then calculated using eq 2.

sphere and using the calibration results from the reference sphere we can determine the displacement of the moving sphere from the position of maximum intensity, as shown Figure 1.

In the experiment, we first use the reference particle to obtain a calibration curve of intensity as a function of displacement from the position of maximum intensity. The focal plane of the objective is then adjusted to lie between the maximum intensity positions for the reference sphere and moving spheres.

By measuring the intensities associated with the reference sphere and the moving spheres the displacement from the midplane of the gap, z, can be obtained from the calibration curves according to the formula

$$z = L/2 - \Delta s_r - \Delta s_m - \sigma/2 \qquad (2)$$

where σ is the particle diameter, Δs_r and Δs_m are the displacements from the position of maximum intensity of the reference and moving spheres, respectively, and L is the gap thickness. Again, the situation is illustrated in Figure 1.

Typically, 1−6 particles are tracked together, including the reference particle, with a total of about 7−12 particles tracked for each gap. Each tracking run consists of 100 data points per particle and lasts approximately 10 s. At each time the x and y coordinates (dimensions parallel to the plates) and intensity are stored for each particle.

For each gap thickness, an intensity-displacement calibration curve is generated for the reference sphere,

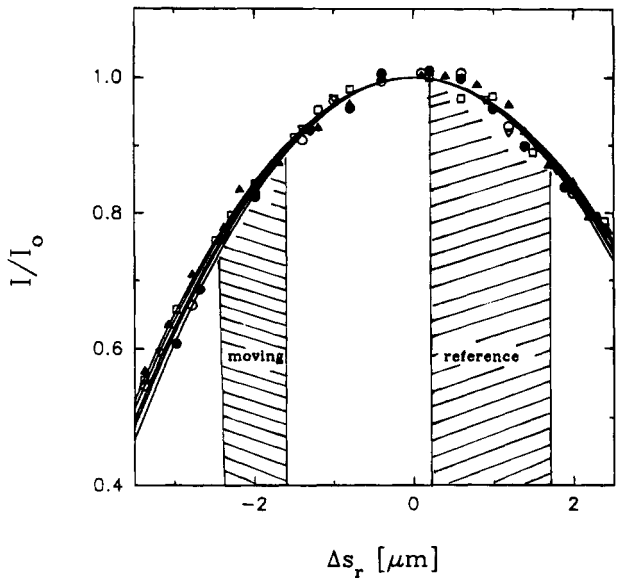

Figure 2. Calibration curves of the normalized intensity (I/I_o) vs displacement from the position of maximum intensity for five different gaps between glass plates: 4.0 μm (hollow circles), 5.0 μm (hollow triangles), 6.2 μm (hollow squares), 7.2 μm (solid triangles), and 8.4 μm (solid circles). I_o values are obtained from parabolic fits to the data, $I = I_o - A\Delta s_r^2$ (solid lines). Also shown are the typical ranges of displacement values for the reference and moving particles.

followed by tracking of the intensities of the moving and reference spheres, and finally a thickness measurement of the gap.

Calibration Procedure

Because the stage micrometer of the microscope provides only a coarse measure of the stage displacements, a linear variable differential transformer (LVDT) is used to measure the stage-height motion for small displacements. The coils of the transformer are mounted on the body of the microscope, while the core piece is attached to the stage. A PAR-122 lock-in amplifier drives the primary coil of the LVDT and analyzes the output from the secondary coils. Voltage readings are taken from a digital voltmeter attached to the output of the lock-in amplifier. A calibration of the LVDT voltage readings with the stage height motion gave a linear curve, with a slope of 14.9 μm/V.

To calibrate the intensity of the reference particle to the LVDT voltage readings, the focus of the microscope was adjusted so that at least one pixel of the reference sphere appears above the threshold value and the average intensity and LVDT voltage are recorded. This is repeated as the focus is adjusted through the position of maximum particle intensity and on until there are no more pixels above the threshold value. During calibration the stage micrometer is only advanced in one direction thus avoiding any backlash in the gears.

The resulting intensity−voltage curves can be converted to intensity−displacement curves by using the results of the calibration of the stage height to the LVDT voltage readings. Besides the 14.9 μm/V conversion factor, an additional factor of 1.33 is needed to correct for the difference between the index of refraction in the cell (water) and the index of refraction outside the cell (air).

The results are shown in Figure 2, where the intensity is plotted as a function of the displacement from the position of maximum intensity. Also plotted are parabolic fits to the data of the form $I = I_o - A\Delta s_r^2$. The value of I_o is not the same for all calibration curves due to adjustments of the light source intensity between data sets, but the normalized curves (I/I_o) are very similar. In fact, the calibration procedure should be independent of the size of the gap, and the variation among the calibration curves gives an estimate of the error associated with using them for measuring the sphere displacements. For the typical range of displacements (shown in Figure 2) the measurements of $\Delta s = \Delta s_r + \Delta s_m$ (used in eq 2) are expected to be accurate to within 0.07 μm.

Results

Once the intensity−displacement calibration curve is obtained, moving spheres are tracked along with the reference sphere, as described above. By using the intensity values recorded for the moving and reference spheres, along with the calibration curves of Figure 2, the sphere displacement from the midplane can be obtained according to eq 2.

Before these calculations are made however, it is necessary to make some modifications to the data. Because of fluctuations of the light source, the reference particle intensity distributions are not δ functions. These fluctuations will also affect the intensity of the moving spheres. Therefore, at each time step, t, the fluctuations are corrected according to the formula, $I_{new}(t) = I_{old}(t)\langle I_{ref}\rangle / I_{ref}(t)$, where $I_{new}(t)$ and $I_{old}(t)$ are, respectively, the corrected and measured values of the intensity of the moving sphere, $I_{ref}(t)$ is the measured value of the reference sphere intensity, and $\langle I_{ref}\rangle$ is the intensity of the reference particle averaged over the time of the tracking run.

In addition, there are also inhomogeneities in the background illumination of the field of view, with the center being the brightest and most uniform region. To avoid spurious results from inhomogeneities in the field of view, the reference spheres are located in the middle region, and a cutoff radius around the reference sphere is used to reject the data points of any moving sphere that goes beyond this radius. In order to insure that the spheres are isolated from each other, data points are also rejected if any pair of spheres is separated by less than four sphere diameters.

The resulting distributions, using the screening criteria, the intensity correction, and eq 2, are shown in Figure 3, where the probability distribution for displacement from the midplane is plotted for each gap thickness. It can be seen that the distributions broaden as the gap is increased, as one would expect, but that the positions of the peaks vary about the midplane, and that this variation does not change consistently as the gap is changed.

The histograms in Figure 3 are expected to be a good approximation of the equilibrium distribution at each value of the gap thickness. As described previously, the data in the figure comes from tracking many independent spheres (approximately 10 s each), and each sphere will independently be sampling the equilibrium distribution. In all cases, except for the largest gap, the time for a sphere to diffuse the width of the distribution is smaller than the time over which a single sphere is tracked.

The accuracy of the measurements of z can be estimated from the error in the terms used to calculate it (eq 2). As discussed earlier, the measurements of L are expected to be accurate to within 0.14 μm, and the accuracy in $\Delta s = \Delta s_r + \Delta s_m$ is approximately 0.07 μm. The variance of the diameter of the spheres is typically less than 2%, and not large enough to add any significant error. Of all the sources of error, inaccuracies in the measurement of the gap thickness would most directly contribute to errors in the location of the spheres relative to the midplane of the gap. From eq 2 it can be seen that errors in the

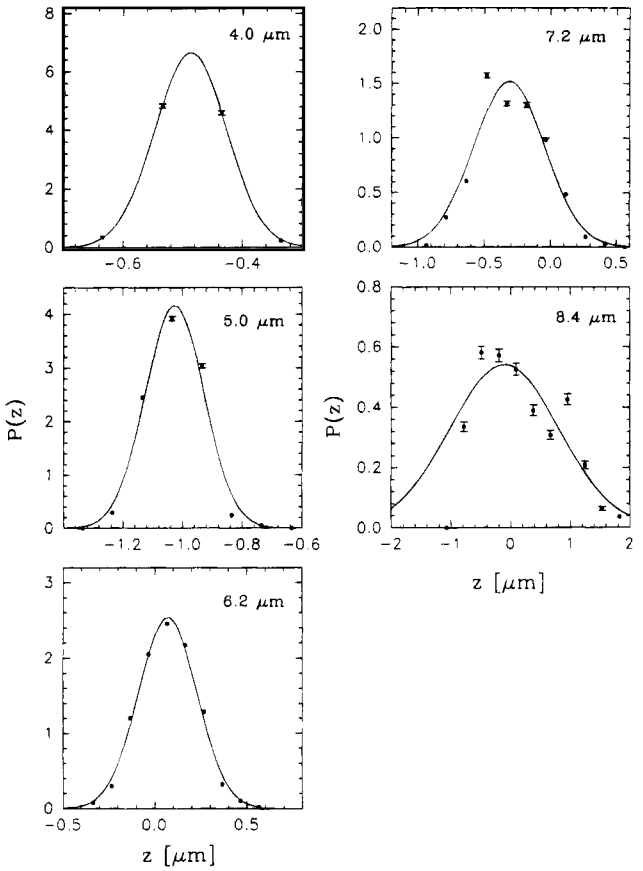

Figure 3. Normalized probability distributions [$P(z)$] of displacement (z) from the midplane for five different gaps obtained from experimental data (circles). Also shown (solid lines) are curves obtained by fitting the experimental data to Gaussian probability distributions. Fitted parameters are shown in Table 1.

measurement of the gap would systematically shift the distribution of sphere positions relative to the midplane of the gap. However, the size of the gap measurement errors is not large enough to entirely account for the those distributions that are centered well off the midplane of the gap. The other sources of error are not correlated and are also not large enough to account for the shifted distributions.

The variation in the positions of the distributions relative to the midplane of the gap could be due to variations in the surface charge of the plates. Because it is necessary to move the cell in order to change the gap and make a thickness measurement, each data set is taken at a different place on the post. If there are variations in the surface charge of the plates, the charge of the top and bottom plates may not be equal, and there will be variations in the position of the spheres relative to the midplane of the gap. Another observation that supports the hypothesis that the charge is asymmetric is that all the stuck spheres used to obtain the reference intensity discussed in the Calibration Procedure section adhered to the small glass post and not the larger microscope slide.

DLVO Analysis

The theory of double-layer repulsion and van der Waals attraction formulated by Derjaguin, Landau, Verwey, and Overbeek (DLVO) can be used to describe the interaction between the plates and a sphere. In this case, the van der Waals attraction will be ignored, since the spheres and plates are dissimilar materials, and with the low ion concentration of the dispersion the contribution of any attractive van der Waals force would be negligible. At the distance of closest approach the attractive potential between sphere and plate is estimated to be less than 0.1 k_BT (less than 0.1% of the estimated repulsive force at the same separation).

The repulsive Coulomb potential between a sphere and a plate can be written as[7]

$$V_R = B \ln(1 + e^{-\kappa\sigma(x-0.5)}) \tag{3}$$

where $B = 32\pi\epsilon\epsilon_0\sigma\gamma_s\gamma_p(k_BT/e)^2$, the subscripts s and p refer to the sphere and plate respectively, $\gamma = \tanh(e\psi_o/4k_BT)$, ψ_o is the appropriate surface potential for the sphere or plate, σ the particle diameter, κ is the inverse Debye screening length, e is the electron charge, and $x = r/\sigma$, where r is the distance from the sphere center to the plate. Equation 4 applies for the case of monovalent counterions and large $\kappa\sigma$. There are separate equations for the case of small $\kappa\sigma$, and this experiment, with $\kappa\sigma$ approximately three, lies somewhere between the two extremes. The expression for the small $\kappa\sigma$ case is quite complicated, however, and will not be considered here.

For a sphere confined between two plates,

$$V_R = B_1 \ln(1 + e^{-\kappa\sigma(x_1-0.5)}) + B_2 \ln(1 + e^{-\kappa\sigma(x_2-0.5)}) \tag{4}$$

where the subscripts 1 and 2 refer to the top and bottom plates respectively, which in general can have different surface potentials. Making the change of coordinates $x_1 = (L/2 - (z - z_o) - z_o)/\sigma$ and $x_2 = (L/2 + (z - z_o) + z_o)/\sigma$

$$V_R = B_1 \ln(1 + ae^{\kappa z_o}e^{\kappa(z-z_o)}) + B_2 \ln(1 + ae^{-\kappa z_o}e^{-\kappa(z-z_o)}) \tag{5}$$

where $a = \exp(-\kappa(L - \sigma)/2)$, and z_o is the position of the potential minimum.

For the conditions of this experiment, the exponential terms within the logarithms are small enough that the approximation $\ln(1 + u) = u$ can be used and

$$V_R = a(B_1e^{\kappa z_o}e^{\kappa(z-z_o)} + B_2e^{-\kappa z_o}e^{-\kappa(z-z_o)}) \tag{6}$$

Expanding the exponentials and keeping terms up to second order gives

$$V_R = 2aB_{eq}(1 + \kappa^2(z - z_o)^2/2) \tag{7}$$

where $B_{eq} = B_1 \exp(\kappa z_o)$, and we have made use of the fact that the minimum of the potential occurs at z_o and $B_1 \exp(\kappa z_o) = B_2 \exp(-\kappa z_o)$.

To second order then, the repulsive potential felt by the spheres can be approximated as a harmonic potential, and the resulting distribution curve will be a Gaussian. Figure 3 shows the results of fitting the data to a Gaussian distribution[1]

$$P(z) = P_o e^{-[(z-z_o)/\sigma_z]^2/2} \tag{8}$$

where $P(z)$ is the probability of finding the particle at a distance z from the midplane, and the fitted Gaussian parameters are summarized in Table 1. The Gaussian distributions seem to fit the data well except for the 8.4-μm data, where the experimental distribution drops off prematurely as the particle moves below the midplane.

(7) Verwey, E. J.; Overbeek, J. Th. G. *Theory of the Stability of Lyophobic Colloids*; Elsevier: New York, 1948.

Table 1. Gaussian Parameters for Particle Displacement Distributions

data set	gap (μm)	P_o	σ_z (μm)	z_o (μm)	B_1/B_2	ω (m s^{-1})
a	4.0	6.7	0.060	−0.49	6.5	32
b	5.0	4.2	0.099	−1.02	51	19
c	6.2	2.5	0.16	0.07	0.76	12
d	7.2	1.5	0.27	−0.31	3.3	7.7
e	8.4	0.54	0.92	−0.10	1.5	2.1

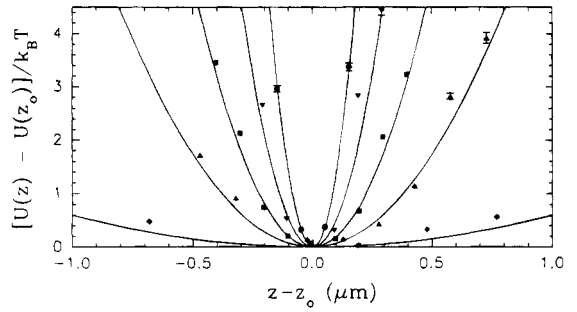

Figure 4. The dimensionless interaction potential relative to the minimum potential energy $[U(z) - U(z_o)]/kT$, between a single colloidal sphere and two glass plates is shown as a function of displacement from the equilibrium position (z_o), for several spacings between the plates. The potentials were obtained from the distributions of Figure 3 using $\ln[P(z)] = \ln(C) - U(z)/k_BT$ (eq 9). The constant C was chosen such that $\ln(C) = U(z_o)/k_BT$, with z_o the particle's equilibrium position. Experimental data (symbols) is shown: 4.0 μm (circles), 5.0 μm (downward triangles), 6.2 μm (squares), 7.2 μm (upward triangles), and 8.4 μm (diamonds), along with fits to a harmonic potential (solid lines).

As the gap increases the harmonic approximation will eventually become inadequate. In the limit of large gap, the particle diffuses essentially as a free particle in the central region of the gap, and only feels the repulsive potential close to the glass surface. The data set for the 8.4-μm gap approaches such a case.

From eq 1

$$\ln(P(z)) = \ln(C) - U(z)/k_BT \qquad (9)$$

Thus the measurement of $P(z)$ yields the potential energy to within a constant. Since the potential energy itself is only defined to within a constant, we define the minimum value of the potential to be zero, which occurs at $z = z_o$. In Figure 4 the dimensionless potential energies, $[U(z) - U(z_o)]/kT$, are plotted for each of the different gaps. The potentials are well fit by a quadratic function, indicating the harmonic approximation to the potential is accurate.

The equipartition theorem applied to a harmonic oscillator with spring constant k, predicts that $k\langle(z-z_o)^2\rangle = k_BT$, and for the Gaussian distribution of eq 9, we have $\langle(z-z_o)^2\rangle = \sigma_z^2$. Using the results of the Gaussian fits we can test how well the data fits the DLVO theory by comparison with eq 8. From this comparison, we would expect $2aB_{eq}\kappa^2 = k_BT/\sigma_z^2$. Figure 5 shows the result of fitting $2aB_{eq}\kappa^2/k_BT$ to the σ_z data obtained from the Gaussian fits, as a function of the gap thickness L. The theory predicts that σ_z^2 varies exponentially with the plate spacing, L. Except for the largest gap, the results are fit well by a single value of the screening length, $\kappa^{-1} = 0.52$ μm, a value consistent with the presence of ion exchange resin in the sample. The fit also yields $2B_{eq}/k_BT = 1.0 \times 10^3$. If the surface potentials of the sphere and plates are the same, this would imply a value of 20 mV for the surface potential.

It has been noted that the sphere distributions are not centered at the midplane of the gap, indicating an anisotropy in the charge of the plates. Although the pre-

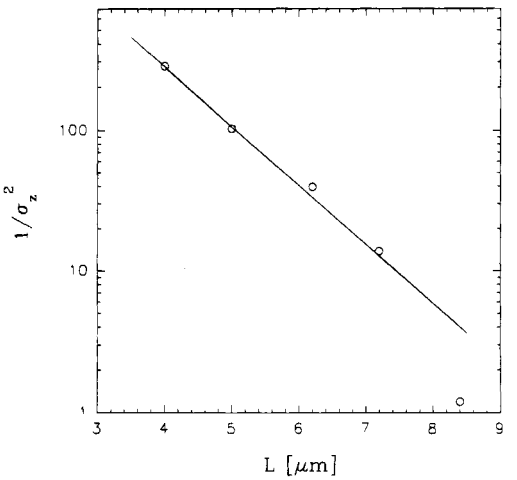

Figure 5. The inverse square of the width of the distributions shown in Figure 3 ($1/\sigma_z^2$) vs gap spacing. The circles are data and the solid line is a fit to a harmonic approximation of the DLVO theory for sphere−plate interactions. The fitted parameters from eqs 8 and 9 are $\kappa^{-1} = 0.52$ μm and $2B_{eq}/kT = 1.0 \times 10^3$.

experimental cleaning of the cover glass and post are the same, the manufacture of the two is different. The cover glass is cut from standard microscope slide glass (borosilicate), while the small post is cut to order from plates of BK-7 glass. It is also possible that residual films on the glass might locally reduce the surface charge of either of the glass surfaces. The anisotropy in the strength of the two surfaces is given by $B_1/B_2 = \exp(-2\kappa z_o)$. These values are also shown in Table 1.

Langevin Oscillator

The motion of a sphere perpendicular to the plates can be approximated as that of a one-dimensional harmonic oscillator undergoing Brownian motion. The motion is described by the Langevin equation

$$d^2z/dt^2 = -\beta\, dz/dt + A(t) - \omega^2 z \qquad (10)$$

where m is the mass of a sphere, $\beta = f/m = 3\pi\eta\sigma C/m$ is the viscous relaxation rate, f is the friction coefficient, $A(t)$ is the stochastic acceleration, η is the viscosity, σ is the sphere diameter, C is a correction factor that accounts for the reduced diffusion coefficient of the spheres in the narrow gaps, and ω is the natural frequency of the oscillator, related to the spring constant by $k = m\omega^2$. The correction factor is the ratio of the free diffusion coefficient to the reduced diffusivity caused by wall effects and is a function of the sphere radius and gap thickness,[5] ranging from 1.2 to 1.7 for this experiment. The friction does not affect the equilibrium distribution function of sphere positions, which is independent of dissipative processes, but does affect the time, τ, necessary for the equilibrium distribution to be obtained.

The solutions to this problem have been worked out by Chandrasekhar,[1] Uhlenbeck and Ornstein,[8] and Wang and Uhlenbeck,[9] and depend upon the quantity $\beta_1^2 = \beta^2 - 4\omega^2$, with β_1 real corresponding to overdamped motion, β_1 imaginary for periodic motion, and β_1 zero corresponding to aperiodic motion. However, in the limit of large βt for the periodic and aperiodic cases, or large $(\beta - \beta_1)t$ for the overdamped case, all the solutions have the same form, and the second moment is $\langle(z-z_o)^2\rangle = k_BT/m\omega^2$. The equipartition result is approached exponentially with a

(8) Uhlenbeck, G. E.; Ornstein, L. S. *Phys. Rev.* **1930**, *36*, 823.
(9) Wang, M. C.; Uhlenbeck, G. E. *Rev. Mod. Phys.* **1945**, *17*, 323.

time constant of $\tau = f/k$, which is the ratio of the friction coefficient to the spring constant. For our case $\beta = (1.3-1.6) \times 10^7\ s^{-1}$, and we can assume the limiting case of large βt applies, calculate ω, and then calculate β_1 to verify if the assumption is correct.

The ω values derived from the experimental data are shown in Table 1. Since the ω values are small compared to β, the equation for β_1 can be rewritten as $\beta_1 = \beta(1 - 2\omega^2/\beta^2)$. From this expression it can be seen that β_1 is real and we are dealing with the overdamped case. In addition, $1.6 \times 10^{-2}\ s < \tau < 3\ s$. The appropriate time constant for the approach to equilibrium is given by τ. Since tracking of a single particle takes approximately 10 s, the assumption of t/τ large is valid and a proper ensemble average of the displacement distribution is obtained.

Conclusion

Video microscopy techniques have been used to track the movement of polystyrene spheres perpendicular to the confining glass plates in a 2D geometry. From these measurements we have obtained probability distributions for the position of the spheres, relative to the midplane of the gap, for five different plate spacings and have determined the sphere−plate potential energy. The rms displacement of the spheres increases exponentially as the gap between the plates is increased. The most probable position for the spheres varies and is not always located at the midplane, possibly indicating spatial charge variation on the glass surfaces. The broadening of the sphere distributions as the gap is increased is consistent with a harmonic approximation to the DLVO theory using only screened electrostatic forces and ignoring attractive Van der Waals forces. It is shown that the experimental situation can be described in terms of an overdamped Langevin oscillator and that our measurements are long enough to ensure that a proper statistical ensemble is obtained. Our model produces reasonable values for the Debye screening length and surface potentials of the sphere and glass plate.

Acknowledgment. This research was supported by NSF DMR-459850 and DOE DE-FG02-87ER45084. We thank Prof. R. B. Meyer for encouragement and numerous discussions.